

# Impact of the non-repeatability of sources and receivers in ocean bottom acquisitions - a synthetic 2D study in Santos Basin Pre-salt

Filipe Borges, Mônica Muzzette, Luiz Eduardo Queiroz, Bruno Pereira-Dias, Roberto Dias and André Bulcão

Petróleo Brasileiro S. A. (Petrobras)

Copyright 2021, SBGf - Sociedade Brasileira de Geofísica.

This paper was prepared for presentation at 17<sup>th</sup> International Congress of the Brazilian Geophysical Society, held in Rio de Janeiro, Brazil, 8-11 November, 2021.

Contents of this paper were reviewed by the Technical Committee of the 17<sup>th</sup> International Congress of The Brazilian Geophysical Society and do not necessarily represent any position of the SBGf, its officers or members. Electronic reproduction or storage of any part of this paper for commercial purposes without the written consent of the Brazilian Geophysical Society is prohibited.

## Abstract

**Time-lapse seismic feasibility studies support acquisition and processing planning, being also essential for a good 4D interpretation. In this work, we study the effects of source and receiver non-repeatability in time-lapse acquisitions with ocean bottom sensors. We perform 2D acoustic seismic modeling with high-resolution property models in two distinct dates. To simulate source and receiver non-repeatability, different acquisition geometries are considered for each vintage. The synthetic data are compared in terms of time-lapse amplitude and time-shifts, and repeatability is quantified via the normalized root mean squared attribute (NRMS). For the parameters considered in our study, the deterioration of NRMS seems to be dominated by the non-repeatability of the receivers, with source non-repeatability having a lower contribution. We believe the results presented in this work are a first step towards a more robust methodology for time-lapse feasibility studies, which incorporate imaging uncertainties.**

## Introduction

Time-lapse seismic is the most common geophysical solution for reservoir monitoring (Johnston, 2013). As seismic acquisition and processing improve in quality, more detailed features can be extracted from the data. Hence, the demand for continuous improvement in time-lapse seismic quality calls for ever-higher repeatability - our capacity of reproducing exactly, in the monitor acquisition, the same parameters of the baseline. This becomes even more critical for reservoirs with low 4D signal, like the Brazilian pre-salt reservoirs in Santos Basin (Cypriano et al., 2019).

In this work, we used 2D finite differences (FD) full wave modeling to estimate the effect of non-repeatability of sources and receivers in time-lapse ocean bottom nodes (OBN) acquisitions. Highly detailed acoustic property models, incorporating flow simulation of a pre-salt field, were created for the baseline and monitor scenarios, and several geometry combinations were investigated. Random noise, calibrated to field experiments, was also added to the data. The time-lapse effect was analyzed

using time-lapse amplitude, time-shifts and normalized root mean square (NRMS) attribute as selected criteria for comparison. In the modeled scenarios, the deterioration of NRMS was dominated by random noise and by the non-repeatability of the sources, with receivers non-repeatability playing a secondary role. The evaluation of several configurations was only possible because 2D modeling times were drastically reduced with the current GPU implementation of the finite differences code - such analysis would be very time-consuming in 3D, as a total of five scenarios had to be modeled and imaged.

## Method

In this section we discuss model building, modeling algorithm, and survey geometries. We highlight that the area selected for this study is a pre-salt oil field located in Santos Basin, offshore Brazil, with carbonate reservoirs of Aptian age. Due to confidentiality constraints, the data presented in this work was de-characterized.

The available seismic data in the area was reverse time migrated, and the migration velocity model was available for this study. An arbitrary inline section from this data was selected for this study. The migrated depth section can be seen in Figure 1. The horizons mapped in green are the top and base of the salt layer. The salt thickness varies expressively in the area. Besides, salt properties are not homogeneous, as can be seen by the internal reflections - this characteristic plays an important role in properly imaging those areas (Maul, 2020).

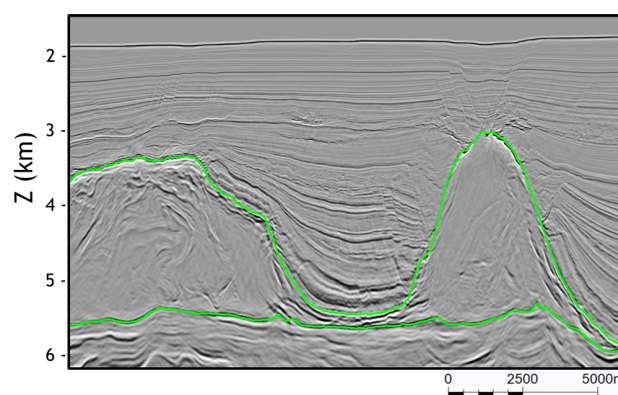


Figure 1: Seismic section in the study area. Green lines represent the top of salt (ToS) and base of salt (BoS) horizons.

### Model Building

The velocity model used for migration of the image in Figure 1 is quite smooth, and hence not adequate for finite difference modeling, mainly because the lack of seismic reflections that would be generated due to the low contrast between layers (Schuster, 2017). Using the available data, high-resolution models of P-wave velocity and density were built. For that step, the model was divided in three regions: post-salt overburden, salt layer, and reservoir.

For the post-salt sediments, the smooth migration velocity was combined with the migrated seismic data to create a higher-frequency P-wave velocity volume. Then, an empirical equation (Gardner et al., 1974) was applied to the resulting P-wave velocity model, yielding a high-resolution density model for the post-salt sediments.

In the salt layer, a different approach was employed, based on the use of seismic inversion for salt characterization. An acoustic inversion yields a volume of P-wave impedance for the salt. Then, a proprietary empirical relation was applied to this acoustic impedance volume, resulting in the density property. More details about this methodology can be found in Teixeira and Lupinacci (2019).

Acoustic properties in the reservoir layers were estimated with the help of a petroelastic model (PEM), since this is the layer that will undergo changes between baseline and monitor surveys. The rock properties were obtained from well logs, calibrated by laboratory ultrasonic measurements and analysis of rock mineralogy. The hydrocarbon properties were obtained via analysis of sampled reservoir fluid, while brine properties were calculated using the results published by Batzle and Wang (1992). Fluid saturation and pressure in the baseline and monitor dates were obtained from flow simulation.

The combination of all steps above yields the final volumes of density and P-wave velocity. Figure 2 compares the initial velocity model, used for migration, to the final velocity used for forward modeling in the baseline scenario. The density for this scenario is also shown (Figure 2c). The original migration velocity is kept for all migrations (baseline and monitor) that were performed with the modeled data.

### Survey Geometry

The main goal of this work is to investigate the effect of source and receiver non-repeatability in time-lapse data. Two parameters were selected to be examined: uncertainty in sources position and uncertainty in receivers position. Starting from a typical parametrization of 50 m source spacing (close to the sea surface) and 500 m receiver spacing (at the seabottom), the variables are changing according to the described below:

**Uncertainty in source position** Uncertainty in source position was modeled as a random variable following a normal distribution of zero mean, and two scenarios for standard deviation: 0 (perfect repeatability) or 5 m. The value of 5 m was the result of the statistical analysis of previous OBN acquisitions in the area of interest. This uncertainty applies only to horizontal displacements - source depth was kept fixed at 8 m.

**Uncertainty in receiver position** Like in the source position, the uncertainty for the receivers are

modeled in two scenarios as a random variable with normal distribution of zero mean and standard deviations of either 0 (perfect repeatability) or 5 m. These numbers were also based on analysis of the previous surveys in the area of study. The depth of the receivers is the same of the sea bottom in their location, and in this study no depth uncertainty was assumed for the positioning.

Figure 3 zooms in into the implementation of source and receiver uncertainties. The geometry scenarios are created by starting with a regular grid and disturbing it using a random deviation for sources and receivers. This process was performed independently for baseline and monitor surveys. Notice how neither spacing remains regular, and that they are distinct between surveys. Since the position errors in sources (dS) and receivers (dR) from baseline to monitor are the difference between two zero mean, normally-distributed random variables, they also follow a normal distribution with zero mean, but a standard deviation increased by a factor of  $\sqrt{2}$  (Figure 3c).

Following those assumptions, two realizations were independently generated for sources and receivers. We will use the mnemonics S1 and R1 for the positions of source and receivers in the realization 1, and S2 and R2 for realization 2. The baseline vintage is always modeled with the geometry S1R1, and the geometry of the monitor vintage can vary. There are four possible geometry combinations, described below:

**Perfect Repeatability (S1R1-S1R1)** Both sources and receivers positions are kept the same for baseline and monitor surveys, i.e., the perturbed (non-regular) geometry of baseline survey is repeated for monitor. This scenario is used as benchmark.

**Non-repeatable Receiver (S1R1-S1R2)** Sources are kept at the same positions in baseline and monitor surveys (same realization - S1), but receiver positions change (R1 on baseline and R2 on monitor). The aim of this scenario is to isolate the effect of receiver non-repeatability. It can also be interpreted as an OBN field experiment in which, despite the uncertainty in receiver positioning, the dense shooting grid allows for perfect reconstruction of a regular source grid, leading to perfect repeatability on the source position between baseline and monitor vintages.

**Non-repeatable Source (S1R1-S2R1)** Sources are at different positions in each survey (different realizations - S1 for baseline, S2 for monitor), but receivers are repeated (same realization R1). The purpose of this scenario is to isolate the effect of source non-repeatability. It can be thought of as a permanent reservoir monitoring (PRM) geometry, where the receivers are perfectly repeated in the baseline and monitor surveys, but there is some uncertainty in source position.

**Non-repeatable Geometry (S1R1-S2R2)** The whole geometry is different between acquisitions (different realizations for sources and receivers positions - S1R1 and S2R2). It is the situation that is closest to a ocean bottom nodes (OBN) field experiment,

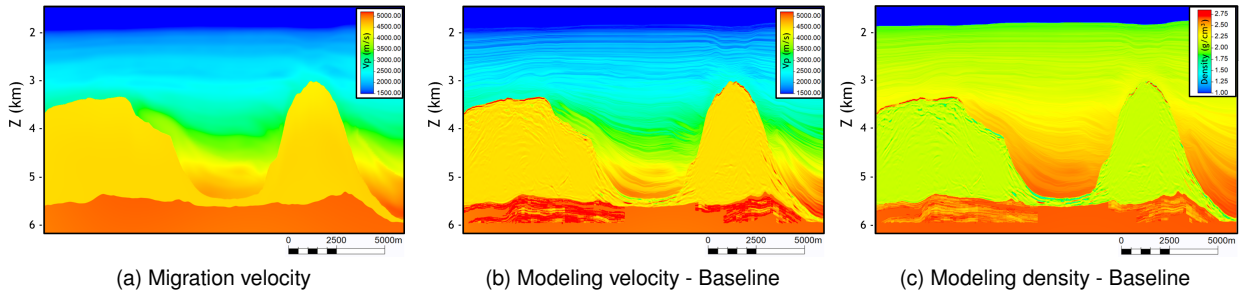


Figure 2: Property models used for imaging (all scenarios) and forward FD modeling (baseline scenario).

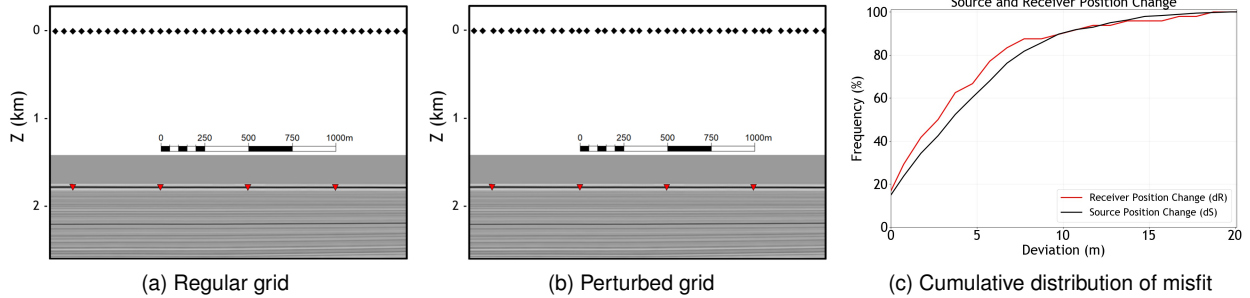


Figure 3: Comparison of regular (a) and non-perturbed (b) grids, applying a normally-distributed perturbation to both sources and receivers. Black diamonds represent the sources (at 8 m depth), and red triangles are the receivers (at the sea bottom). Panel (c) shows the cumulative distribution of the misfit for receivers (dR - red) and sources (dS - black) between baseline and monitor.

if no improvement can be achieved in the source positioning during processing.

The geometries described above, together with the property models, are the inputs for the finite difference (FD) modeling, which we detail in the next section.

#### FD Modelling and Imaging

Forward modeling was performed using an implementation of the non-linear two-way acoustic isotropic wave equation with variable density (Schuster, 2017). The wavelet selected for modeling was a Butterworth with maximum frequency of 80 Hz. The modeled wavefield is registered with a 4 milliseconds sampling, and the grid size is 5 m x 5 m. Since the number of receivers is one order of magnitude lower than that of sources, reciprocity was used, and the receiver positions were treated as sources during the seismic modeling and migration process. This was done purely for practical reasons and in the text we refer to source and receiver without the reciprocity “trick”.

After forward modeling, white Gaussian noise was added to the seismograms. The noise level was selected to match field recordings of OBN data in the area. The synthetic seismograms were then used as input for a reverse time migration (RTM), performed with the same migration velocity used in the field data (Figure 2a). The migration velocity was the same regardless of geometry scenario or vintage being modeled. Prior to migration, a mute on the direct wave is applied. Data was modeled without source or receiver ghost, and only the upgoing wave field was migrated this analysis.

#### Time-lapse amplitude, time-shift and NRMS

The quantitative metric selected in this study to evaluate the quality of the time-lapse data was the normalized root mean square (NRMS), whose formula is shown below:

$$\text{NRMS} = 200 \times \frac{\text{RMS}_{\text{Monitor} - \text{Baseline}}}{\text{RMS}_{\text{Baseline}} + \text{RMS}_{\text{Monitor}}} \quad (1)$$

There is some discussion on the literature about the use of NRMS as a repeatability metric, particularly concerning data of different frequency content (Lecerf et al., 2015) or in the occurrence of time-shifts (Cantillo, 2012). To circumvent those discussions, we chose to model all scenarios with the same frequency content, and the NRMS was calculated around the top and base of salt (ToS and BoS) horizons, using a window of 40 meters (9 samples). Because there are no modeled geomechanical effects nor production outside the reservoir layers, no time-shift is expected above the reservoir, so the NRMS metric for this horizon should be a fair one to compare the scenarios.

For effects of display on the results section, all 4D amplitudes  $\Delta A_{4D}$  are calculated subtracting the baseline data from the monitor data:  $\Delta A_{4D} = A_{\text{Monitor}} - A_{\text{Baseline}}$ .

For time-shift computation, the migrated depth images were converted to time using the same velocity model adopted in the RTM. Then, time-shifts were computed by finding the lag associated with the maximum cross-correlation value between monitor and baseline data, on a trace-by-trace basis ( $\Delta t_{4D} = t_{\text{Monitor}} - t_{\text{Baseline}}$ ). The cross-correlation was computed in a 128 ms moving window, with

steps of one sample (4 ms). The vertical axis was taken as positive in the downward direction, so a positive time-shift means that the monitor seismic is displaced towards later times, when compared to the baseline data.

The color convention used for time-lapse amplitudes and time-shifts follows the standards proposed by Stammeijer and Hatchell (2014), with warm colors representing *softening* and cold colors representing *hardening*.

## Results

Figure 4 shows a comparison of some modeled seismograms (receiver gathers). All plots were generated for the same receiver, but for different configurations. Figure 4a is from the baseline scenario. Figure 4b is the time-lapse seismogram in the scenario of perfect repeatability, while Figure 4c shows the situation with uncertainties in both sources and receivers. No random noise was added to those seismograms. The 4D seismograms have a color scale ten times tighter.

Figure 5 compares a migrated section from the 3D field data (see Figure 1) and the 2D synthetic data (modeled and migrated) for the baseline scenario. The similarity is striking, despite the lack of the sea floor reflection, since only the upgoing wavefield was selected for imaging.

Figure 6 shows 4D amplitude data (monitor minus baseline) and time-shifts for some modeled scenarios. The 4D amplitudes were obtained by raw difference between the baseline and monitor vintages - no warping to align the reflectors was applied. The relative acoustic impedance change is also plotted (Figure 6a). The theoretical zero-offset time-shifts, calculated as the difference between the integrated slowness of each vintage, is shown in Figure 6b. Table 1 compiles the values of NRMS calculated for the modeled scenarios.

Table 1: NRMS values at top of salt (upper table) and base of salt (lower table) horizons for the 4 modeled geometries, with and without addition of white Gaussian noise (WGN).

WGN	S1R1-S1R1	S1R1-S1R2	S1R1-S2R1	S1R1-S2R2
No	-	1.89	1.19	2.39
Yes	1.61	2.58	2.27	3.04

WGN	S1R1-S1R1	S1R1-S1R2	S1R1-S2R1	S1R1-S2R2
No	-	1.53 %	1.39 %	2.23 %
Yes	2.89 %	3.32 %	3.47 %	3.95 %

## Discussions

We start by discussing the remarkable similarity between 3D field and 2D synthetic data (Figure 5). The full wave acoustic modeling, combined with high-resolution property models, was able to deliver a 2D migrated depth image comparable to the 3D real dataset. This is a qualitative sign of the robustness of the model building methodology, as well as of the FD modeling and migration algorithms.

The time-lapse seismograms shown in Figure 4 are a visual representation of coherent noise caused by non-repeatability: mispositioning between baseline and monitor surveys leads to the appearance of “noise”, but - on

synthetic cases - only where there is data on either vintage. This type of noise, usually proportional to the 3D reflections amplitude, might be challenging to mitigate during 4D pre-processing. In Figure 4b, only the 4D signal is visible.

Figure 6 visually summarizes this study. The time-lapse amplitudes and time-shifts can be seen for all scenarios. As in Figure 4, non-repeatability of sources and receivers causes coherent 4D noise, which can be seen in Figure 6e as a noise that almost tracks the strong reflectors, like the salt shape. This noise undermines our ability to identify and isolate the 4D anomalies that are clearly seen in the perfect geometry scenario (Figure 6c). The inclusion of random noise (Figure 6e) further deteriorates the time-lapse amplitude responses.

A similar analysis can be made for the time-shifts. As expected, non-repeatability and random noise degrade the calculated time-shifts. It was surprising to us that, even in the benchmark scenario (Figure 6d), the obtained time-shifts are fairly different from the theoretical values (Figure 6b). This might be due to the lack of pre-conditioning of data prior to cross-correlation.

The NRMS values shown in Table 1 indicate that, for the parameters used in this study, sources mispositioning and random noise were the factors that contributed the most to hinder the repeatability, with receivers uncertainty playing a lesser role. The parameters selected in this work (geometry uncertainty, noise levels) aimed at reproducing field data acquired in the area of study, therefore leading us to conclude that they are adequate to quantifying the contribution of each factor to the total NRMS. An analysis performed with different parameters might of course lead to a different conclusion, which does not invalidate the results presented here.

No dedicated 4D processing has been applied to the data prior to computation of the time-lapse attributes. Although source mispositioning had a strong effect on NRMS for our study, our experience with processing of field data in the receiver domain shows that a dense shooting grid allows for a good wavefield reconstruction in a regular grid, which could severely reduce this non-repeatability impact. Since in practice the sources can be better handled during processing (and also because currently there are no engineering solutions for achieving actual perfect repeatability on the source side), the focus of reducing the NRMS should be on improving receiver repeatability - via PRM systems, for example. While the differences in the values in Table 1 seem small, even a minor NRMS improvement can significantly expand our ability to detect the time-lapse signal in the area (Mello et al., 2019).

Lastly, we highlight that one important aspect of non-repeatability in offshore seismic was not addressed in this study: water velocity variations. It is well documented that the speed of sound in the water layer changes seasonally. These changes alter the propagation of seismic waves, having consequences in time-lapse analysis (Han et al., 2012). This is a clear next step for our work.

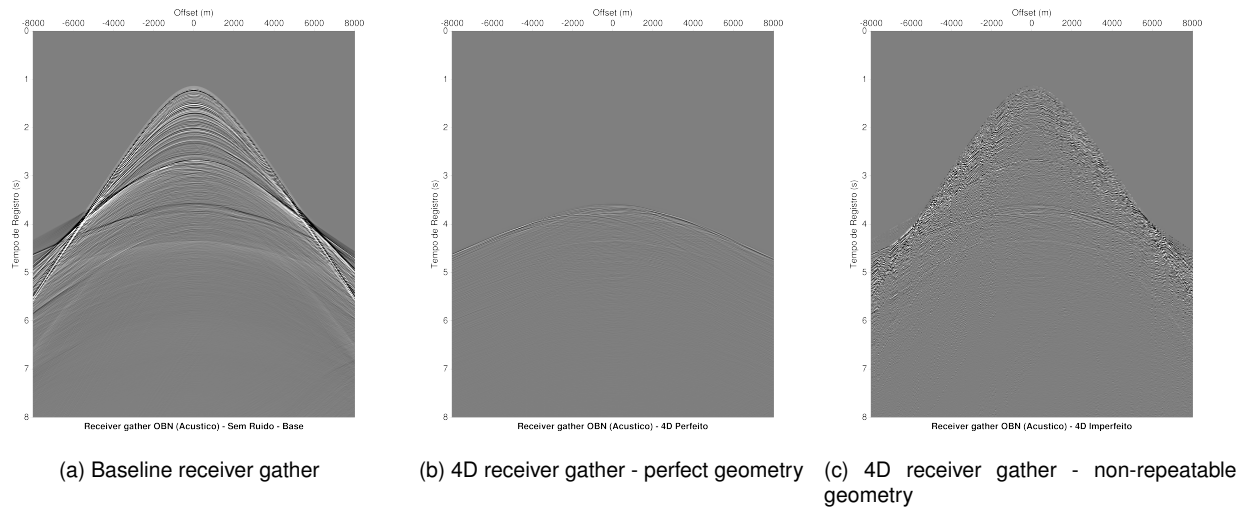


Figure 4: Receiver gather of baseline scenarios (a) and 4D difference of seismograms with repeatable (S1R1-S1R1) and non-repeatable (S1R1-S2R2) geometry scenarios - (b) and (c), respectively. Color scale in time-lapse seismograms is ten times tighter.

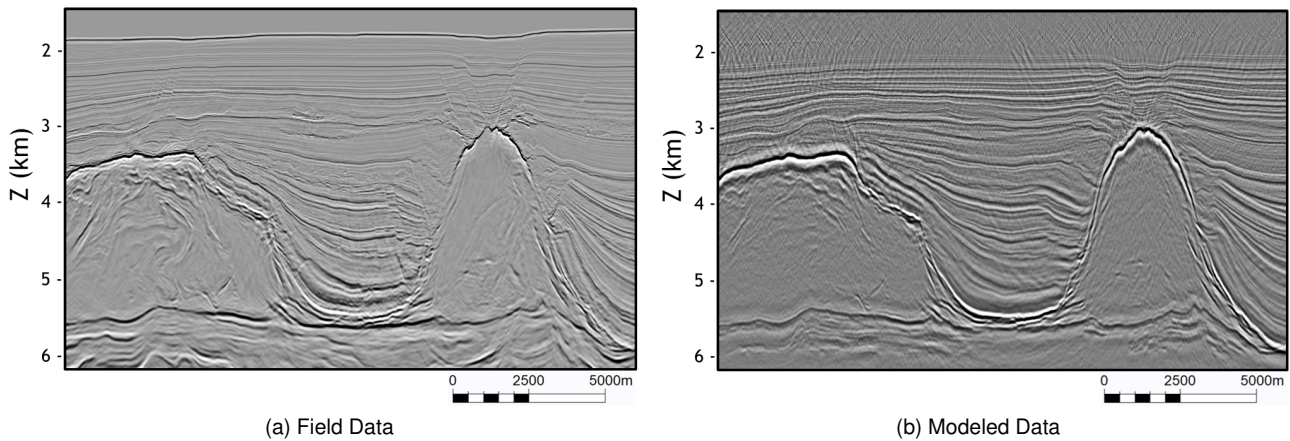


Figure 5: Comparison between the field (a) and synthetic (b) migrated sections in the study area. Modeled data is from the baseline scenario.

## Conclusions

We analyzed non-repeatability of synthetic ocean bottom seismic data, considering the contribution of random noise and geometry uncertainty. Seismic images for baseline and monitor vintages were generated using 2D high-resolution property models from a pre-salt field in Santos Basin, full wave modeling and RTM. The synthetic data were compared in terms of time-lapse amplitude and time-shift. The results indicate that, in the lack of dedicated 4D processing, the NRMS is dominated by random noise and by non-repeatability of the receivers, with source mispositioning playing a secondary role. Because the expected time-lapse signal from pre-salt reservoirs is fairly low, any improvements in source and receiver positioning can be decisive to measure it.

## Acknowledgments

We would like to thank Petróleo Brasileiro S.A. (Petrobras) for financial support to develop this study, as well as for the permission to publish the results.

## References

- Batzle, M., and Z. Wang, 1992, Seismic properties of pore fluids: *Geophysics*, **57**, 1396–1408.
- Cantillo, J., 2012, Throwing a new light on time-lapse technology, metrics and 4d repeatability with sdr: *The Leading Edge*, **31**, 405–413.
- Cypriano, L., Z. Yu, D. Ferreira, B. Huard, R. Pereira, F. Jouno, A. Khalil, E. N. A. Urasaki, N. M. S. M. da Cruz, A. Yin, D. Clarke, and C. C. Jesus, 2019, Obn for pre-salt imaging and reservoir monitoring – potential and road ahead: Presented at the 16th International Congress of the Brazilian Geophysical Society & EXPOGEF 2019, Rio de Janeiro, Rio de Janeiro, Brazil.
- Gardner, G., L. Gardner, and A. Gregory, 1974, Formation velocity and density—the diagnostic basics for stratigraphic traps: *Geophysics*, **39**, 770–780.
- Han, F.-X., J.-G. Sun, and K. Wang, 2012, The influence of sea water velocity variation on seismic traveltimes, ray paths, and amplitude: *Applied Geophysics*, **9**, 319–325.
- Johnston, D., 2013, Making a difference with 4d:

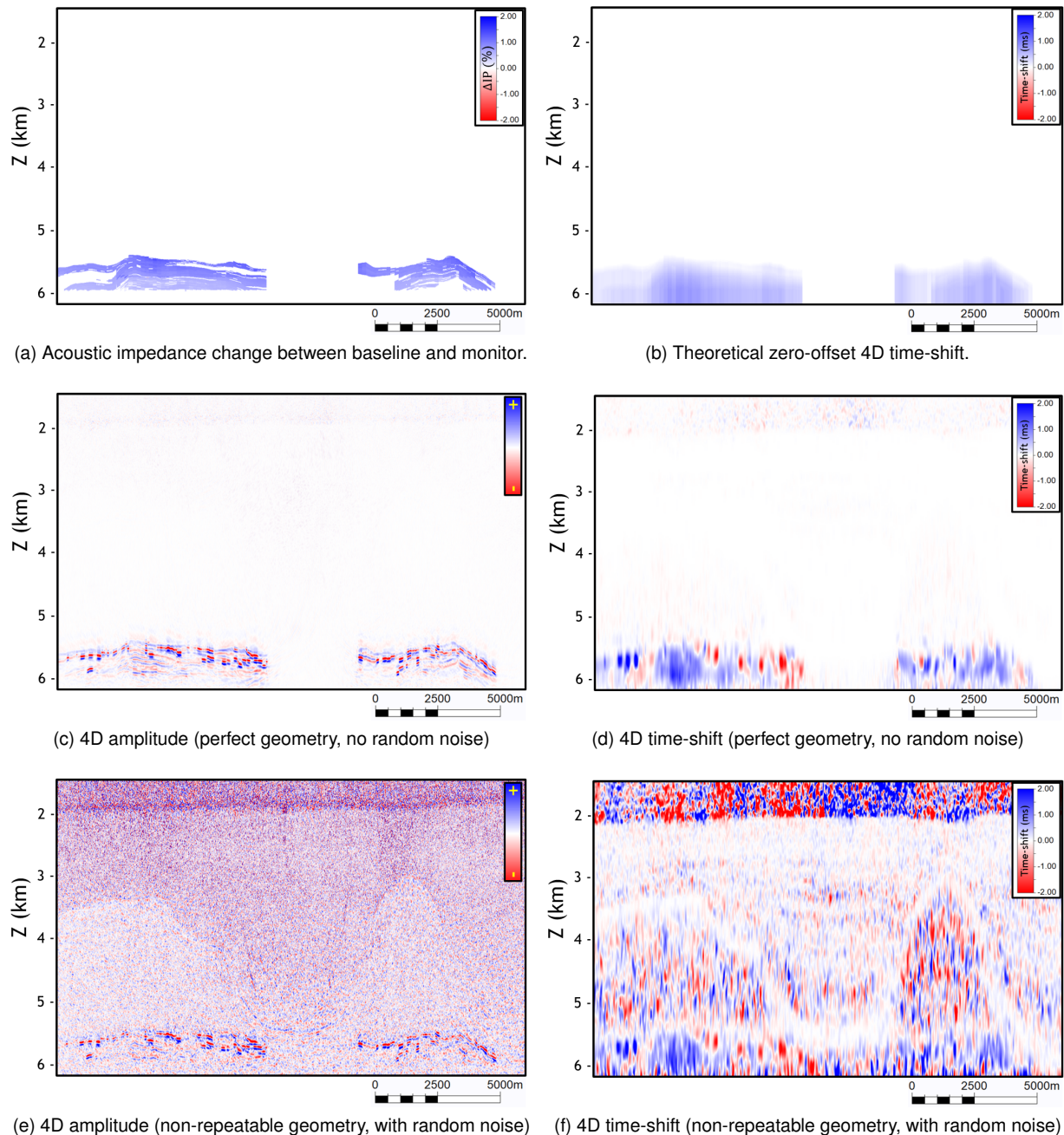


Figure 6: Comparison of time-lapse amplitude and time-shifts for the modeled scenarios. First row shows modeled acoustic impedance change (a) and theoretical zero-offset time-shift (b). Second row shows results for perfect repeatability geometry, and third row for non-repeatable geometry with Gaussian white noise.

practical applications of time-lapse seismic data: SEG distinguished instructor short course 2013.

Lecerf, D., J. Burren, E. Hodges, and C. Barros, 2015, Repeatability measure for broadband 4d seismic, *in* SEG Technical Program Expanded Abstracts 2015: Society of Exploration Geophysicists, 5483–5487.

Maul, A., 2020, Caracterização sísmica das estratificações da seção evaporítica salina e suas aplicações nos projetos de exploração, desenvolvimento e produção de hidrocarbonetos: PhD dissertation, UFF.

Mello, V., M. Santos, R. Penna, J. Rosseto, and C. Deplante, 2019, 4d petroelastic modeling for a brazilian

pre-salt field: What to expect from interpretation?: 81st EAGE Conference and Exhibition 2019, European Association of Geoscientists & Engineers, 1–5.

Schuster, G. T., 2017, Seismic inversion: Society of Exploration Geophysicists.

Stammeijer, J., and P. Hatchell, 2014, Standards in 4d feasibility and interpretation: *The Leading Edge*, **33**, 134–140.

Teixeira, L., and W. M. Lupinacci, 2019, Elastic properties of rock salt in the santos basin: Relations and spatial predictions: *Journal of Petroleum Science and Engineering*, **180**, 215–230.